Kiprotich, S. et al. (2018). Effect of growth temperature on the structural, optical and luminescence properties of cadmium telluride nanoparticles. Journal of Materials Science: Materials in Electronics, 1-8
http://dx.doi.org/10.1007/s10854-018-8574-6

Effect of growth temperature on the structural, optical and luminescence properties of cadmium telluride nanoparticles

Sharon Kiprotich, Martin O. Onani and Francis B. Dejene

Abstract

Cadmium telluride (CdTe) has been successfully prepared by a simple wet chemical process at different reaction temperatures. Temperature is one parameter that thermodynamically plays an important role in controlling the growth rate, morphology, size and size distribution of the as-prepared nanoparticles (NPs). Effect of this parameter was investigated on the growth, structural and optical properties of CdTe NPs. It was observed that the Powder X-ray diffraction (XRD) pattern for samples prepared at 50 °C had many impurities from unreacted precursors while those prepared at > 100 °C displayed polycrystalline NPs. The XRD results revealed that the structure of the CdTe NPs was cubic with the planes (111), (220), (311) being the main observed peaks. The crystallite sizes obtained from Scherrer formula increased with the increase in growth temperature (2.86–3.62 nm grown at 50–200 °C respectively). The scanning electron microscopy micrographs showed that the morphology of the nanoparticles possessed spherical-shaped particles over the entire surface. This was further confirmed by high resolution transmission electron microscopy micrographs which also displayed increase in the particle size with an increase in the growth temperature. In the optic study, the photoluminescence (PL) spectra displayed a red shift (540–560 nm) in emission as growth temperature increased from 50 to 200 °C. The highest PL peak intensity was realized at a growth temperature of 150 °C. Absorption band maxima were observed to shift towards longer wavelength for higher growth temperatures. The optical band gap decreased with increase in the growth temperature from 2.67 to 2.08 eV for 50–200 °C respectively.

1 Introduction

In the past few decades, exploring novel materials based on semiconductor nanoparticles (NPs) has become one of the most attractive areas of research [1–4]. Studies have been dedicated to the fabrication and characterization of chalcogenide compounds. Cadmium telluride (CdTe) being among these group II–VI compounds, is known to be a good and promising material for the fabrication of various devices such as those applied in optoelectronic, biomedical imaging, nanosensors, photoelectrochemical, electron-beam pumped lasers, solar cells, electroluminescent devices, light emitting diodes etc. [5–10].

As biological luminescent labels, particularly, much attention have been devoted to these semiconductor NPs due to their superior properties like small tunable size, emission tunability, superior photostability, and extended photoluminescence (PL) decay times in comparison to other luminescent organic materials [11–14]. In specific, the CdTe is reported to possess a radioactive recombination of high efficiency, high photosensitivity, high absorption coefficient and direct band gap which correspond to the wide wavelength spectrum from ultraviolet to infrared regions and displaying quantum size effects [15, 16]. The NPs' size and size distribution strongly affect the emission colour and its purity [11–20].With better familiarity regarding the growth of NPs, the colour of emission and colour purity can be controlled to a certain extent so far. When the NPs surface structures are controlled, good PL properties can be obtained which can be used freely for the desired application i.e. its luminescent properties merge well with the biological imaging requirements needed.

The two main existing general approaches for the preparation of NPs are organometallic synthesis using high-temperature precursors [19] and the synthesis in aqueous phase using thiols [21] as capping agents. The most established organometallic synthesis approaches to make crystalline colloidal II–VI NPs [22] is the decomposition of the precursors in high boiling point coordinating solvents such as trioctylphosphine and trioctylphosphine oxide (TOP–TOPO). The organometallic route has been used to prepare CdTe NPs which yielded high PL quantum yields of about 65% at room temperature [23]. However, hindrances of these NPs in many potential applications are the PL instability in air. Nevertheless, aqueous technique is a good alternative to prepare CdTe because the synthetic routes are less expensive, arguably easier to perform, producing more stable NPs which show higher quantum yields than the organometallic counterparts.

In both synthetic routes, the growth temperature is one of the most important parameters which determine the nature of the NPs produced. The size and the structural properties which dictate the luminescence are dependent on this growth temperature. The biological imaging application is a diagnostic tool which is gaining importance in the biological field. The imaging is determined by the luminescence properties of the NPs which ought to be crystalline in nature for desired results. The CdTe must possess desired properties for an application in the biological imaging. This work reports on the investigation of the growth temperature mechanism of the CdTe NPs against their structural and luminescence properties. The CdTe NPs of diff ent sizes, crystallinity, morphologies and PL with enhanced stability were obtained at a low cost by the wet chemical route. Moreover, the CdTe NPs absorb and emit in the range that may not show effects from the body fluids. Interestingly, the method used in this work produces highly crystalline and water soluble CdTe NPs with tunable material properties without performing ligand exchange as reported in most literature.

2 Experimental procedure

The materials used were cadmium acetate dihydrate [Cd $(CH_3COO)_2{\cdot}2H_2O$) (> 99%), to provide cadmium ions, potassium tellurite (K_2TeO_3) (> 90%) which was the source of tellurium ions, l-cysteine (> 98%) as a capping agent and sodium borohydride which was used as reducing agent. All the chemicals used were of analytical grade purchased from Aldrich. Synthesis method was adapted from the literature [24, 25]. Typically, the CdTe QDs was prepared by mixing the proper quantities of cadmium acetate and l-cysteine in a glass beaker. The pH of the solution was then adjusted to 11 by an addition of sodium hydroxide. After that, 50 ml of dissolved 0.2 mmol K_2TeO_3 was added to get an ultimate volume of 100 ml. After stirring for a while, an appropriate amount of sodium borohydride was added to the mixture. The mixture was transferred to a three-necked flask and refluxed at different selected growth temperatures of 50, 100, 150 and 200 °C in open air. Cd: L-Cyst: Te: $NaBH_4$ molar ratios were kept at 1:1:0.5:10.

The crystallographic structure of the CdTe NPs was analysed using a powder X-ray diff actometer with a Cu–Kα radiation (λα = 1.5406 Å) source. The qualitative elemental compositions of the samples were determined by using Oxford Aztec energy dispersive X-ray analysis (EDX) attached to the scanning electron microscope (SEM) equipment. Morphological studies were carried out using a Joel JSM-7800F SEM and the high resolution transmission electron microscope (HRTEM) TECNAI F3OST-TEM model. The UV–Vis analysis were measured at room temperature by using a Shimadzu UV/Vis evolution 100 Spectrophotometer within the wavelength range of 200–1100 nm while photoluminescence measurement was done using Cary Eclipse spectrophotometer; model LS-55 with a built-in 150 W xenon flash lamp.

3 Results and discussion

3.1 Structural and compositional analysis

3.1.1 SEM images

The scanning electron microscopy (SEM) shows the surface topography and composition of a sample. Figure 1 shows the SEM images of CdTe nanocrystals formed at diff rent growth temperatures.

At lower temperature (50 °C), CdTe nanocrystals with nearly spherical shape were formed in groups as shown in Fig. 1a. When the CdTe NPs was grown at temperature of 100 °C, the spherical nanocrystals became uniformly distributed over the entire surface with some rod-like features in them. Increasing the growth temperature further to 200 °C agglomerated spherical shape nanocrystals were observed. The aggregation observed could be a consequence of Ostwald ripening process which is brought about by increase in the supply of thermal energy. Increase in the growth temperature causes an increase in the particle size as shown in Fig. 1. The resulting increase in the particle size is due to the fact that the critical particle radius increases due to disappearance of the smaller particles to enhance the growth of the larger ones [26]. When the reaction temperature is increased from 50 to 200 °C, the morphology of the nanocrystals changes which confirms that the

growth rate of the NPs is sensitive to temperature. Therefore, varying the growth temperature is one of the key ways to control the size and shape of the NPs. However, a growth temperature of produce well dispersed spherical NPs, as can be easily seen in Fig. 1b.

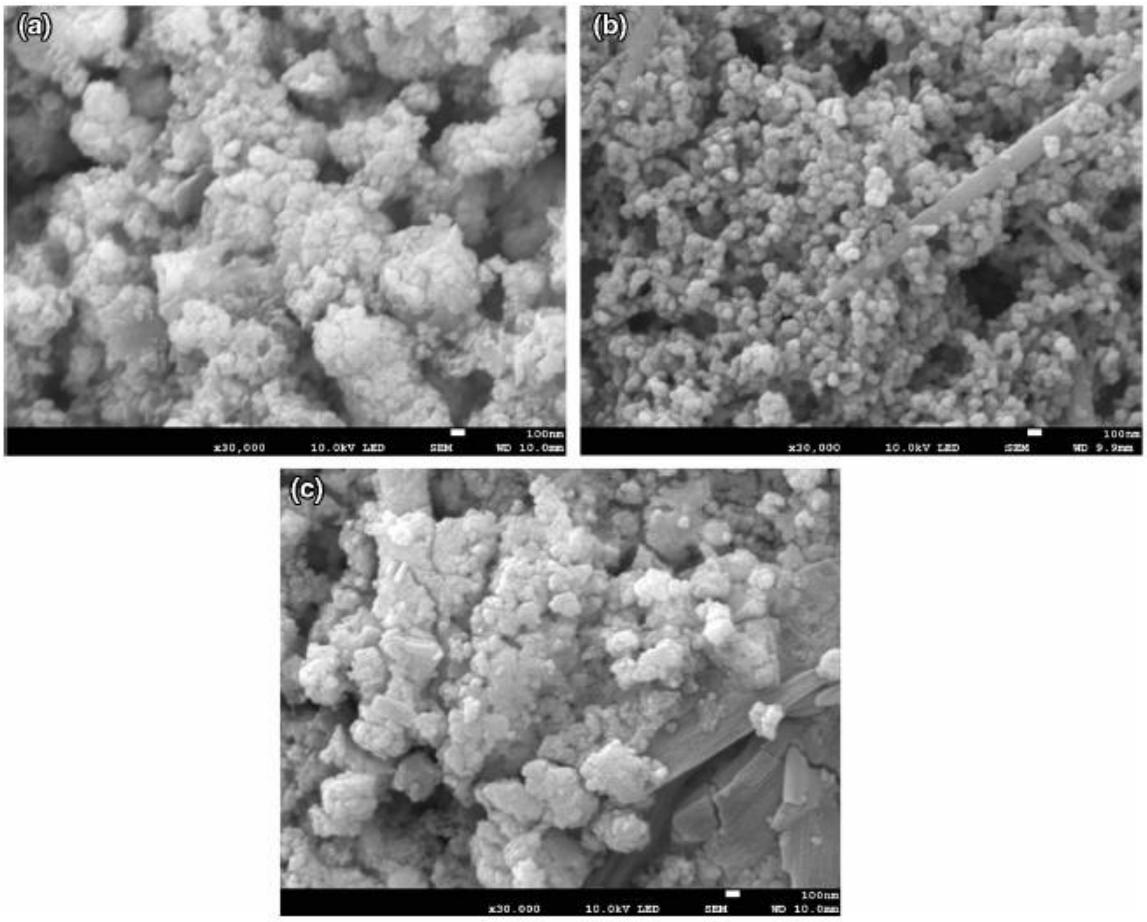

Fig. 1 SEM micrographs of CdTe samples prepared at different growth temperatures (**a** 50 °C, **b** 100 °C and **c** 200 °C)

3.1.2 HRTEM images

The HRTEM images of cysteine capped CdTe NPs are shown in Fig. 2a, b, c, d, e and f. The CdTe nanocrystals are homogeneously distributed and are nearly spherical in shape. The corresponding HRTEM images (Fig. 2d, e and f) show presence of lattice fringes of the nanocrystals. The presence of clearly defined lattice fringes in the HRTEM images describe and confirms the crystalline nature of CdTe NPs. The estimated interplanar lattice spacing of 0.372, 0.373 and 0.376 nm for CdTe NPs grown at 50, 100 and 200 °C respectively were obtained from HRTEM images and can be indexed to the (111) reflections of the cubic phase of CdTe bulk structure. The selected area electron diffraction rings (Insets of Fig. 2a, b and c) also confirmed the crystalline nature of the as-prepared nanoparticles. The average particle sizes were estimated from HRTEM images. Several images were considered when estimating the particle size. A size distribution histogram (Fig. 2g, h and i) was drawn for each set of the CdTe NPs and a Gaussian fit was drawn to give an estimated size of the particle. The obtained particle sizes were 2.76, 3.62 and 5.32 nm for different growth

temperatures as shown in the histogram in (Fig. 2g, h and i). These values compare closely with those estimated from the XRD data.

3.1.3 XRD analysis

The X-ray diff action is a unique technique for determining the crystallinity of a material. The XRD patterns of the as-prepared CdTe samples are displayed in Fig. 3a. Three diff ent peaks are observed which shows that the CdTe samples have zinc blende structures which match well with the standard card no. 75-2086 of bulk CdTe. The XRD peaks correspond to Bragg diff action at (111), (220) and (311) planes of cubic CdTe. The broadened peaks indicate nanocrystalline behaviour and infinitely small size of the CdTe NPs. The values of the full-width half maximum (FWHM) of the XRD peaks were found to increase while the sizes of the nanoparticles decrease and vice versa up to a certain growth temperature (Fig. 3b). The size of the nanoparticles were calculated using the FWHM values of the peak (111) using Debye–Scherer formula [27].The CdTe NPs sizes of all the as-prepared samples were in the range of 2–4 nm.

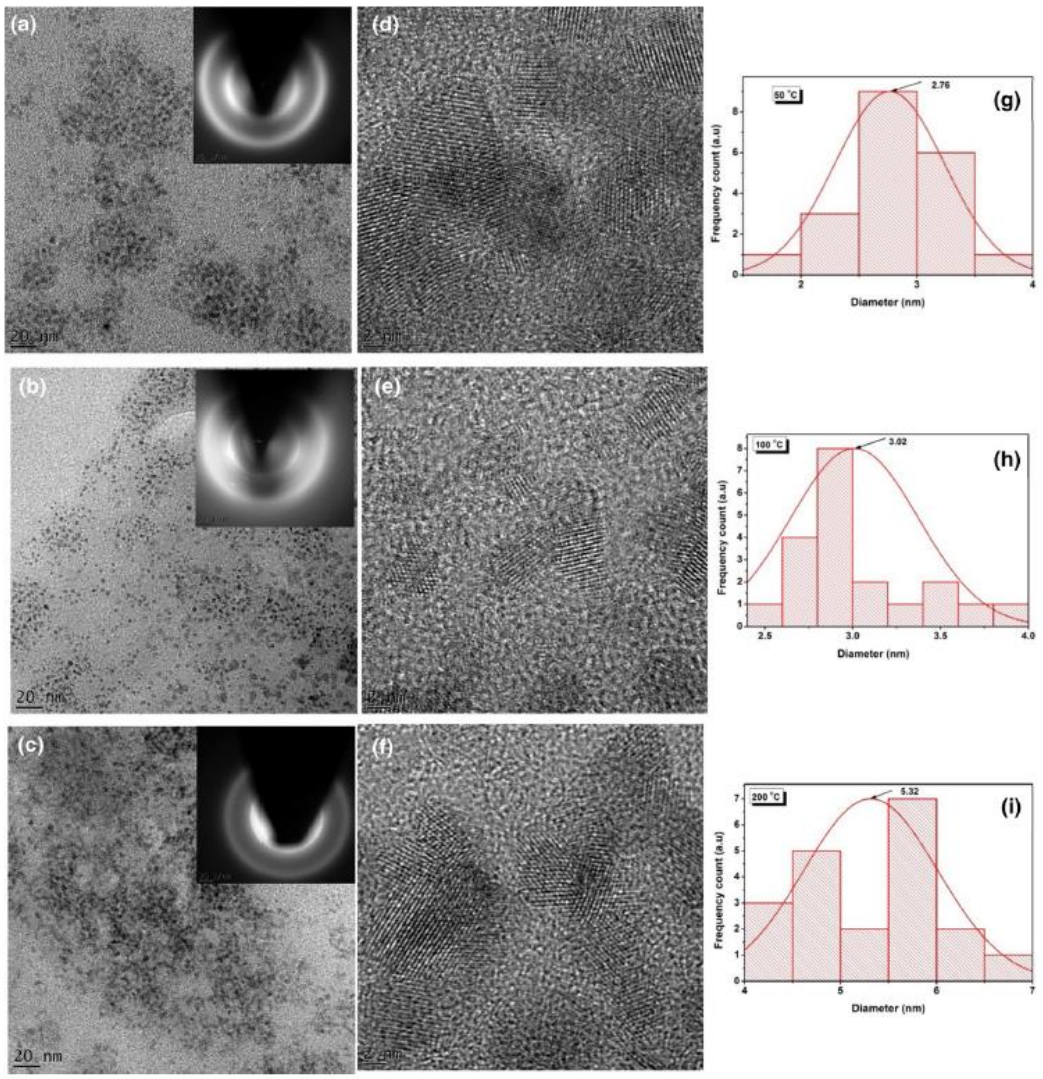

Fig. 2 HRTEM micrographs of CdTe samples prepared at different growth temperatures; **a** 50 °C, **b** 100 °C and **c** 200 °C. Lattice fringes; **d** 50 °C, **e** 100 °C and **f** 200 °C. Size estimates; **g** 50 °C, **h** 100 °C and **i** 200 °C

The calculated average crystallite size values were 2.86, 2.85, 2.74, 2.81 and 3.62 nm for as-prepared CdTe NPs grown at 50, 100, 150, 175 and 200 °C respectively. The constant size realised for the investigated temperature ranges meant that additional points had to be chosen to monitor the trend. Thus the particle size was found to depend so much on the reaction temperature. Increase in the crystallite size indicates the diffusion of smaller particles to form larger ones on increasing the growth temperature. Moreover, increase in crystallite size of the CdTe NPs on increasing the growth temperature confirms the fact that for a stable cubic crystal structure to be formed, a minimum crystallite size is required. From the calculated values (6.35–6.43 Å), lattice constant differs from the standard bulk value (6.41 Å) which is an indication that the nanocrystallites may be under some strain.

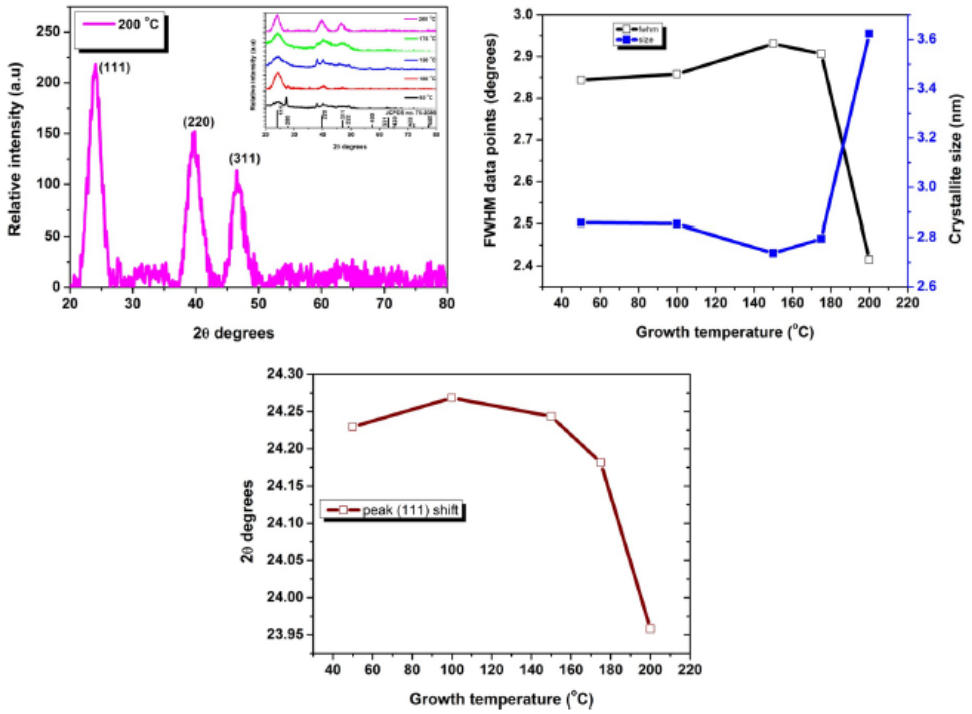

Fig. 3 **a** Representative XRD pattern for CdTe NPs prepared at 200 °C with an inset of XRD patterns grown at different growth temperatures. **b** changes in crystallite sizes and FWHM values of the as-prepared CdTe NPs obtained from XRD pattern peak (111) for different growth temperatures. **c** changes in the peak position of the CdTe NPs XRD peak (111) with growth temperature

The calculation of the strain gives additional information about the structural properties of the CdTe NPs, which can be obtained from the following equation. [28];

$$\varepsilon = \frac{\beta \cos\theta}{4}$$

Where θ is the Bragg's diff action angle, is the strain of the as-prepared CdTe NPs and β is the broadening of the diff action line (FWHM). It is observed that the strain in the as-prepared CdTe NPs increases from 5.972×10^{-1} to 7.163×10^{-1}, with an increase in the growth temperature up to 150 °C. Further increase in the growth temperature decreases

the strain to 5.907×10^{-1}. The increase in strain value is readily ascribed to the increase in defect density or lattice distortion in the CdTe NPs [28].

Figure 3b displays changes in crystallite size and FWHM values of CdTe NPs with growth temperature. It shows that highest peak intensity was obtained at a growth temperature of 100 °C indicating good crystallinity of the sample. Figure 3c depicts changes in XRD peak position for the plane (111) at different growth temperatures. Diff action peaks generally shift to lower diff action angle as growth temperature is increased from 50 to 200 °C. The shift in diffraction peaks was accompanied by a variation in the lattice parameters. The shift in diffraction peaks to lower angle is due to increase in the lattice parameters attributed to lattice expansion.

3.2 Optical properties

3.2.1 Effect on photoluminescence

The optical analysis was studied using spectrophotometer in order to monitor the evolution of nanoparticle growth within a solution. The PL spectra of CdTe NPs grown at various growth temperatures displayed in Fig. 4a show similar PL features. The inset in the Fig. 4a is the normalized PL spectra. It displays clearly the evolution of the PL with various growth temperatures. At the nucleation stage after refluxing at 50 °C, there is a weak luminescence observed from the solution. As the solution heats to 200 °C in about 20 min, the colour of the solution becomes green and finally red. The emission bands could be as a result of the electron–hole recombination. Here, it is observed that increase in the growth temperature causes a red shift in the PL emission wavelengths (522, 533, 561 and 563 nm for 50, 100, 150 and 200 °C respectively) accompanied by variation in the relative intensity.

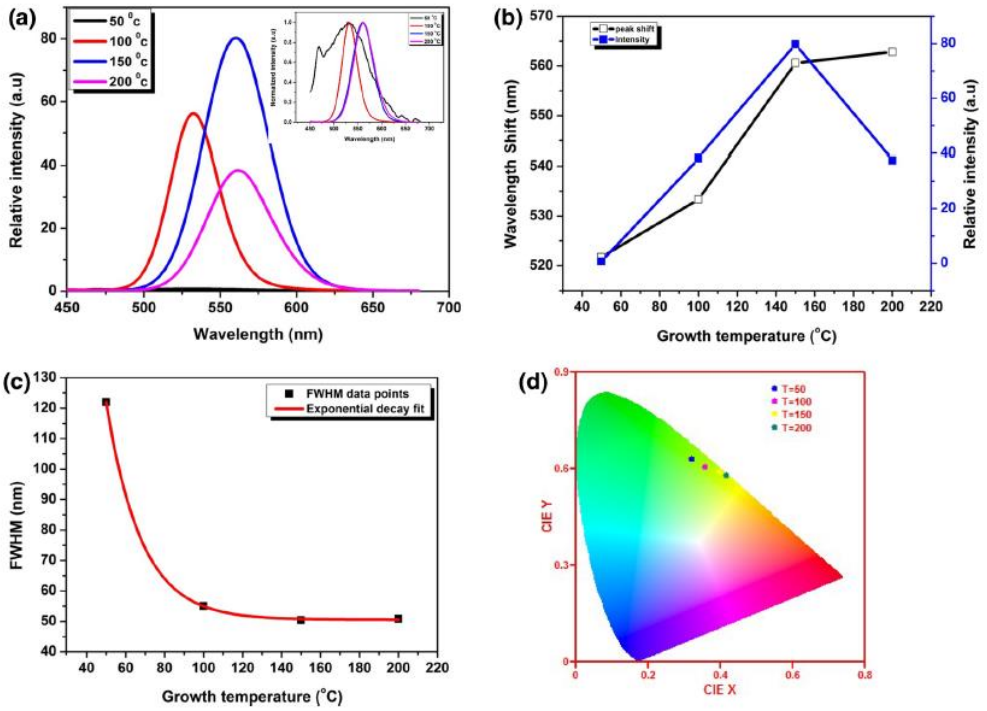

Fig. 4 **a** PL emission spectra and an inset of normalized PL spectra of CdTe NPs prepared at different growth temperatures. **b** changes in peak position and intensity with respect to growth temperature. **c** Exponential curve fit for FWHM data points of as-prepared CdTe NPs at different growth temperatures. **d** CIE image obtained from PL emission data of as-prepared CdTe NPs taken at different growth temperatures

Although not quite clear, the temperature dependent PL, is said to be related to the growth rate mechanism which causes changes in the NPs size for instance, Karczewski et al. [29] found out that with increasing temperature excitons localized in small NPs will dissociate first and then may be captured by neighbouring larger NPs which results in red shift and increase in the luminescence from larger particles formed as small ones are quenched [29]. The aliquot with an emission maximum at 561 nm approached the highest luminescent intensity at 150 °C. The PL intensity increased greatly when the growth temperature is increased and reached a maximum at 150 °C of growth temperature as shown in Fig. 4b. This shows that increasing the growth temperature will enhances the crystal quality of CdTe NPs to a certain extent. The increase in the PL peak intensity could be due to an improved crystallinity of the samples as the growth temperature increases from 50 to 150 °C. It can be concluded that the optimum growing temperature for the CdTe NPs is 150 °C since this gives the highest PL peak intensity showing that the electron hole recombination took place with ease. Omri et al. [30] work suggests that the enhanced intensity could be as a result of low concentration of defects, which act as sites for the non-radiative recombination of electron–hole pairs. The decrease in the PL peak intensity at 200 °C could be due to the sharp decrease in impurities and the surface defects. The crystallinity quality of the CdTe NPs is affected by the decomposition of stabilizer molecules [31, 32] which causes agglomeration as confirmed by SEM and HRTEM images.

The bathochromic shift observed in Fig. 4b is a characteristic nature for nanostructured semiconductors. The results signify that upon an increase in the reaction temperature, the

growth rate of the CdTe NPs is increased. The possible explanation for this behaviour could be that high reaction temperatures cause the growth of larger and irregular NPs with abridged crystallinity due to random, rapid nucleation and with the fast growth affecting the ligand structure of the nanocrystal surface [33]. It should be noted that the red shift in emission peaks supports the reported XRD results of an increase in the diameter of the NPs at higher growth temperatures. It was also observed that the red shift in the PL emission wavelength was due to change in the color of emission with variation in the growth temperature. This phenomenon was further confirmed by the CIE color co-ordinates image shown in Fig. 4d.

3.2.2 Effect on absorbance

Typical absorption spectra of CdTe NPs obtained with different reaction times were given in Fig. 5a. Quantum confinement effects would change the band gaps of NPs with the variation of particle sizes and hence influence the absorption wavelength of the as-prepared samples [34]. From the graph, it is observed that the absorption edges shift to longer wavelength with prolonged growth time. The observed red-shifts of the absorption edges indicated the growth of CdTe NPs during the synthesis hence confirming the PL observation. Absorption band maxima were also observed to shift to longer wavelength for higher growth temperatures. The approximated values of the absorption band maxima were 517, 526, 530 and 332 nm for 50, 100, 150 and 200 °C of growth temperatures respectively. Stokes shift for both green and yellow CdTe nanoparticles is known to be larger for the particles made in open air due to strong phonon coupling [35]. The observed Stoke shift was caused by the band-edge transition due to crystal size distribution [36]. The Stoke shifts for the as-prepared CdTe NPs were 4.9, 7.51, 31.52 and 31.82 nm for 50, 100, 150 and 200 °C.

The increase in the Stoke shift with an increase in growth temperature can be attributed to the fact that nucleation occurs faster at higher growth temperatures and the particles have a high surface area which would lead to a more frequent electron-hole-exchange interaction making the excited-state electron to lose its energy easily resulting in broader stokes shift [37]. The NPs' sizes could be estimated from the UV–Vis absorption spectra using the empirical Eq. (1) [38] where D is the NPs' diameter and λ is the first absorption maximum. The diameters of the CdTe NPs were 2.75, 2.91, 2.97 and 3.00 nm for 50, 100, 150 and 200 °C growth temperatures respectively which are in close agreement to those acquired from XRD studies.

$$D = \left(9.8127 \times 10^{-7}\right)\lambda^3 - \left(1.7147 \times 10^{-3}\right)\lambda^2 + (1.0064)\lambda - 194.84 \quad (1)$$

The absorbance spectra were used to estimate the band gap energies of as-prepared CdTe NPs by using the following Tauc relation for near band-edge optical absorption of semiconductors [39]. The extrapolation of the linear portion of the curve to the X-axis [energy (hv) axis], the intercept gives the value of band gap energy of the as-prepared NPs

(Fig. 5b). The CdTe NPs band gap values were 2.67, 2.50, 2.31 and 2.08 eV for 50, 100, 150 and 200 °C of growth temperature respectively. The band gap values for as-prepared CdTe NPs indicate that as the growth temperature increases, the band gap energy of the NPs decreases. Thus increasing growth temperature increases the size of the NPs hence reducing the optical band gap of the as-prepared NPs.

The Tauc plot of $(Ahv)^2$ versus the photon energy (hυ) for as-prepared CdTe NPs is shown in Fig. 5b. The band gap value of the as-prepared CdTe NPs is shown in Fig. 5b. The observed values are slightly higher than the reported bulk value of 1.5 eV [40]. The shift to higher optical band gap is reported to be attributed to the infinitely small particle size and the subsequent quantum confinement of electronic states in the NPs [2]. In the as-prepared CdTe NPs sample here in reported, the estimated particle size from XRD measurements was about 3 nm and this clarifies the observed large optical band gaps (Fig. 5b) in comparison to the bulk value.

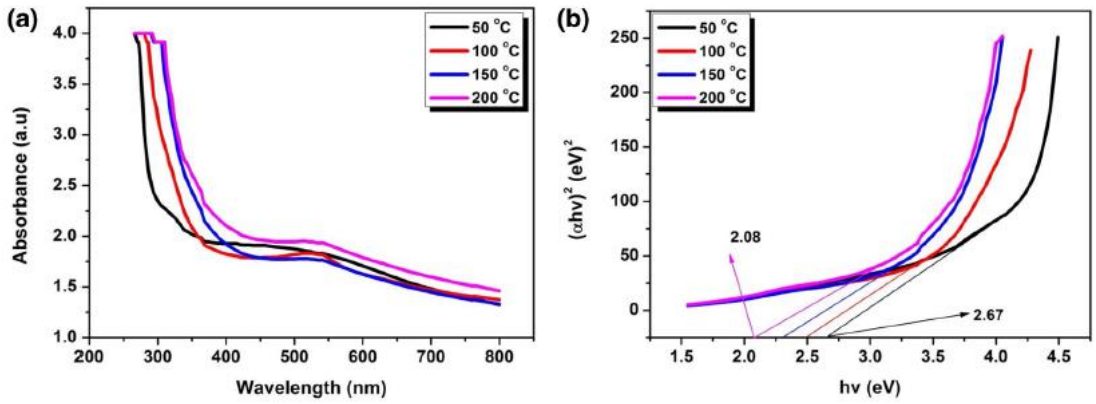

Fig. 5 **a** absorption spectra of CdTe NPs prepared at different growth temperatures. **b** Tauc plot $(\alpha h\nu)^2$ vs. hν to determine the band gap energy of CdTe NPs prepared different growth temperatures

4 Conclusion

The nanoparticles of CdTe were successfully grown by a simple aqueous route at different growth temperatures. The XRD studies revealed the formation of a cubic phase of CdTe nanocrystalline NPs. The average crystallite sizes of CdTe NPs obtained using the Debye–Scherrer equation was found to increase with an increase in the growth temperature (2.86, 2.85, 2.74, 2.81 and 3.62 nm grown at 50, 100, 150, 175 and 200 °C respectively). The SEM analysis on the surface morphology displayed that the micrographs were composed of spherically-shaped NPs uniformly distributed over the entire surface at 100 °C. The HRTEM images displayed spherical particles which confirmed the SEM. The particle sizes estimated from HRTEM images using ImageJ software were in close agreement with the XRD results. The PL analysis displayed a red shift of the emission wave-length with increase in the growth temperature. Highest PL intensity was obtained at 150 °C, an indication of enhanced crystallinity of the sample. UV–Vis analysis showed temperature-dependent properties of the as-prepared CdTe NPs. The absorption edges shifted to longer wavelength as the growth temperature is increased. The estimated optical band gap displayed an inverse

relation with the growth temperature; as the growth temperature was increased, the band gap decreased which is attributed to increase in the particle size. Growth temperature, therefore, is an important parameter for the synthesis of CdTe NPs with tunable material properties. The CdTe NPs prepared at 100 °C using the aqueous technique showed good qualities which are appropriate for biological imaging experiments.

References

1. H. Weller, Angewandte Chem. Int. Ed. Engl. **32**(1), 41–53 (1993) 2. A.P. Alivisatos, Science **271**(5251), 933–937 (1996)
2. J.H. Fendler, Chem. Mater. **13**(10), 3196–3210 (2001)
1. V.I. Klimov, A.A. Mikhailovsky, S. Xu, A. Malko, J.A. Hollingsworth, C.A. Leatherdale, H.-J. Eisler, M.G. Bawendi, Science **290**(5490), 314–317 (2000)
2. N.P. Gaponik, D.V. Talapin, A.L. Rogach, Phy Chem **1**(8), 1787– 1789 (1999)
3. N.P. Gaponik, D.V. Talapin, A.L. Rogach, A. Eychmüller, J. Mater. Chem. **10**(**9**), 2163–2166 (2000)
4. S.V. Gaponenko, A.M. Kapitonov, V.N. Bogomolov, A.V. Prokofiev, A. Eychmüller, A.L. Rogach, Jetp Lett. **68**(2), 142–147 (1998)
5. S.V. Gaponenko, V.N. Bogomolov, E.P. Petrov, A.M. Kapitonov,
6. D.A. Yarotsky, I.I. Kalosha, A.A. Eychmueller, J. Lightwave Technol. **17**(11), 2128–2137 (1999)
7. 9. A. Rogach, A.S.F. Caruso, G. Sukhorukov, A. Kornowski, S. Kershaw, H. Möhwald, A. Eychmüller, H. Weller, Adv. Mater. **12**(5), 333–337 (2000)
8. A.L. Rogach, N.A. Kotov, D.S. Koktysh, J.W. Ostrander, G.A.
9. Ragoisha, Chem. Mater. **12**(9), 2721–2726 (2000)
10. H. Mattoussi, J.M. Mauro, E.R. Goldman, G.P. Anderson, V.C. Sundar, F.V. Mikulec, M.G. Bawendi, J. Am. Chem. Soc. **122**(49), 12142–12150 (2000)
11. X. Gao, Y. Cui, R.M. Levenson, L.W.K. Chung, S. Nie, Nat. Biotechnol. **22**(8), 969–976 (2004)
12. B.J. Battersby, D. Bryant, W. Meutermans, D. Matthews, M.L. Smythe, M. Trau, J. Am. Chem. Soc. **122**(9), 2138–2139 (2000)
13. X. Ding, L. Qu, R. Yang, Y. Zhou, J. Li. J. Luminescence **30**(4), 465–471 (2015)
14. C. Wadia, A.P. Alivisatos, D.M. Kammen, Environm. Sci. Technol. **43**(6), 2072–2077 (2009)
15. R.C. Kainthla, D.K. Pandya, K.L. Chopra, Solid-State Electron.
16. **25**(1), 73–76 (1982)
17. D.V. Talapin, A.L. Rogach, E.V. Shevchenko, A. Kornowski, M. Haase, H. Weller, J. Am. Chem. Soc. **124**(20), 5782–5790 (2002)
18. X. Peng, J. Wickham, A.P. Alivisatos, J. Am. Chem. Soc. **120**(21), 5343–5344 (1998)
19. L. Qu, X. Peng, J. Am. Chem. Soc. **124**(9), 2049–2055 (2002)
20. Z.A. Peng, X. Peng, J. Am. Chem. Soc. **123**(7), 1389–1395 (2001)
21. Z.A. Peng, X. Peng, J. Am. Chem. Soc. **124**(13), 3343–3353 (2002)
22. C.B. Murray, D.J. Norris, M.G. Bawendi, J. Am. Chem. Soc. **115**(19), 8706–8715 (1993)
23. D.V. Talapin, S. Haubold, A.L. Rogach, A. Kornowski, M. Haase, H. Weller, J. Phys. Chem. B **105**(12), 2260–2263 (2001)
24. S. Kiprotich, F.B. Dejene, J. Ungula, M.O. Onani, Physica B **480**, 125–130 (2016)
25. S. Kiprotich, M.O. Onani, F.B. Dejene, Physica B (2017) (In press). https://doi.org/10.1016/j.physb.2017.06.057
26. R.W. Buckley, *Solid state chem research trends*. (Nova Publishers, Hauppauge, 2007)
27. A. Guinier, *X-ray diffraction*. (Freeman, San Francisco, 1963)

28. L.L. Pan, G.Y. Li, S.S. Xiao, L. Zhao, J.S. Lian, J. Mater. Sci.: Mater. Electron. **25**(2), 1003–1012 (2014)
29. G. Karczewski, S. Maćkowski, M. Kutrowski, T. Wojtowicz, J. Kossut, J. Appl. Phys. Lett. **74**(20), 3011–3013 (1999)
30. K. Omri, L. El Mir, Superlattices Microstruct. **70**, 24–32 (2014)
31. K. Omri, O.M. Lemine, L. El Mir, Ceram. Int. **43**(8), 6585–6591 (2017)
32. J. Li, T. Yang, W.H. Chan, M.M.F. Choi, D. Zhao, J. Phys. Chem. C **117**(37), 19175–19181 (2013)
33. M. O'neil, J. Marohn, G. McLendon, J. Phys. Chem. **94**(10), 4356–4363 (1990)
34. W. Guo, J.J. Li, Y.A. Wang, X. Peng, J. Am. Chem. Soc. **125**(13), 3901–3909 (2003)
35. A.P. Alivisatos, T.D. Harris, P.J. Carroll, M.L. Steigerwald, L.E. Brus, J. Chem. Phys. **90**(7), 3463–3468 (1989)
36. A.L. Efros, M. Rosen, M. Kuno, M. Nirmal, D.J. Norris, M. Bawendi, Phys. Rev. B **54**(7), 4843 (1996)
37. C.J. Perez, A.K. Bhattacharjee, M. Chamarro, P. Lavallard, V.D. Petrikov, A.A. Lipovskii, Phys. Rev. B **64**(11), 113303 (2001)
38. W.W. Yu, L. Qu, W. Guo, X. Peng, Chem. Mater. **15**(14), 2854– 2860 (2003)
39. J. Tauc, R. Grigorovici, A. Vancu, Phys. Status Solidi **15**(2), 627–637 (1966)
40. F. Aldeek, L. Balan, J. Lambert, R. Schneider, Nanotechnology **19**(47), 475401 (2008)